Electronic Supplementary Information

for

Mechanism of Molecular Interaction of Acrylate-Polyethylene Glycol Acrylate Copolymers with Calcium Silicate Hydrate Surfaces

Tariq Jamil,[1] Ali Javadi,[2] Hendrik Heinz[1*]

[1] Department of Chemical and Biological Engineering, University of Colorado-Boulder, Boulder, Colorado 80309, USA

[2] Department of Polymer Engineering, University of Akron, Akron, Ohio 44325, USA

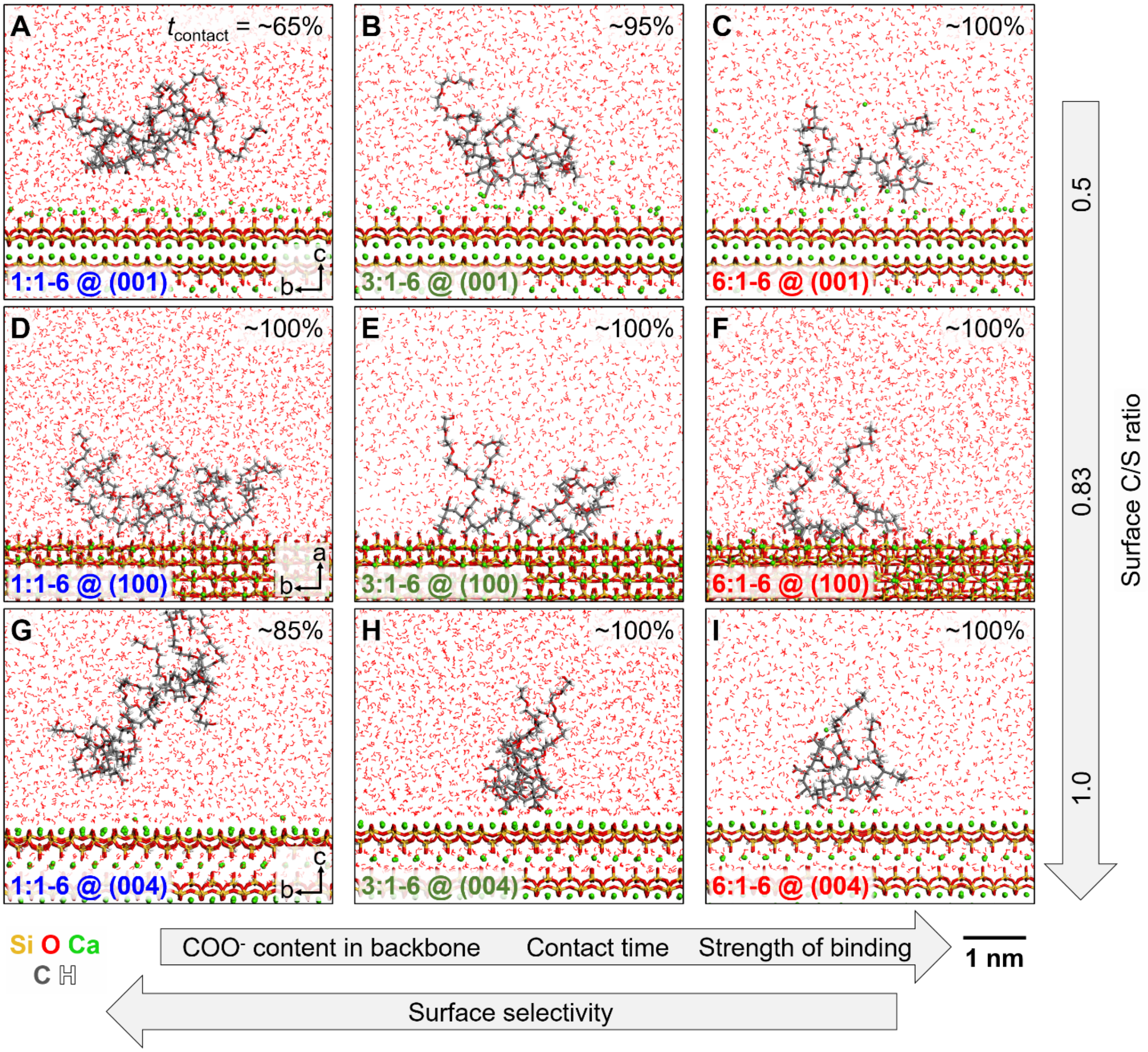

Figure S1. Interaction of PCEs with medium length of side chains with the C-S-H model surfaces. Representative conformations are shown for different surface chemistry and fraction of side chains. (a-c) Representative snapshots and time in contact on the (001) surface of tobermorite 14 Å. As the density of side chains decreases from (a) to (c), contact time with the surface via ionic side groups increases. (d-f) Representative snapshots and time in contact with the (100) surface of tobermorite 14 Å. Contact times are ~100%. (g-i) Representative snapshots and time in contact with the (004) surface of tobermorite 14 Å. Trends in dynamics and interactions are similar to

PCEs with shorter and longer side chains. The contact time is in between the limiting cases (for example in the case of PCE 1:1-6). The height of the simulation boxes was greater than shown for clarity.

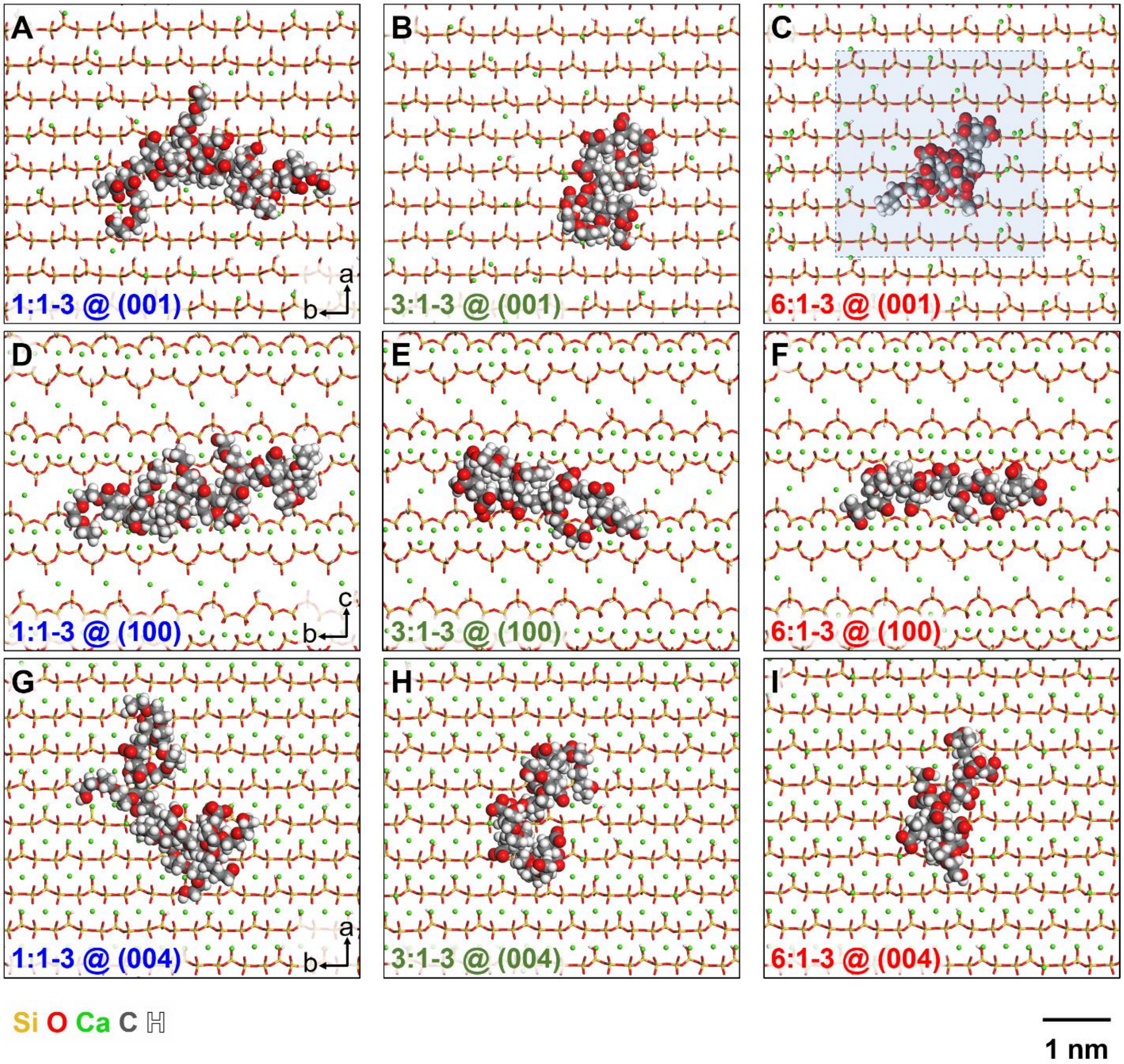

Figure S2. Top view of adsorbed conformation of PCEs with short side chains on the C-S-H model surfaces. Only the first atomic layer of the mineral surface is shown for visual clarity. (a-c) Adsorbed conformations on the (001) surface of tobermorite 14 Å. The blue area in (c) highlights the chosen periodic boundary to maintain constant surface coverage of ~35% relative to PCEs of different compositions. (d-f) Adsorbed conformations on the (100) surface of tobermorite 14 Å. (g-i) Adsorbed conformations with the (004) surface of tobermorite 14 Å. Randomly distributed Ca^{2+} ions between silicate chains originate from the PCEs.

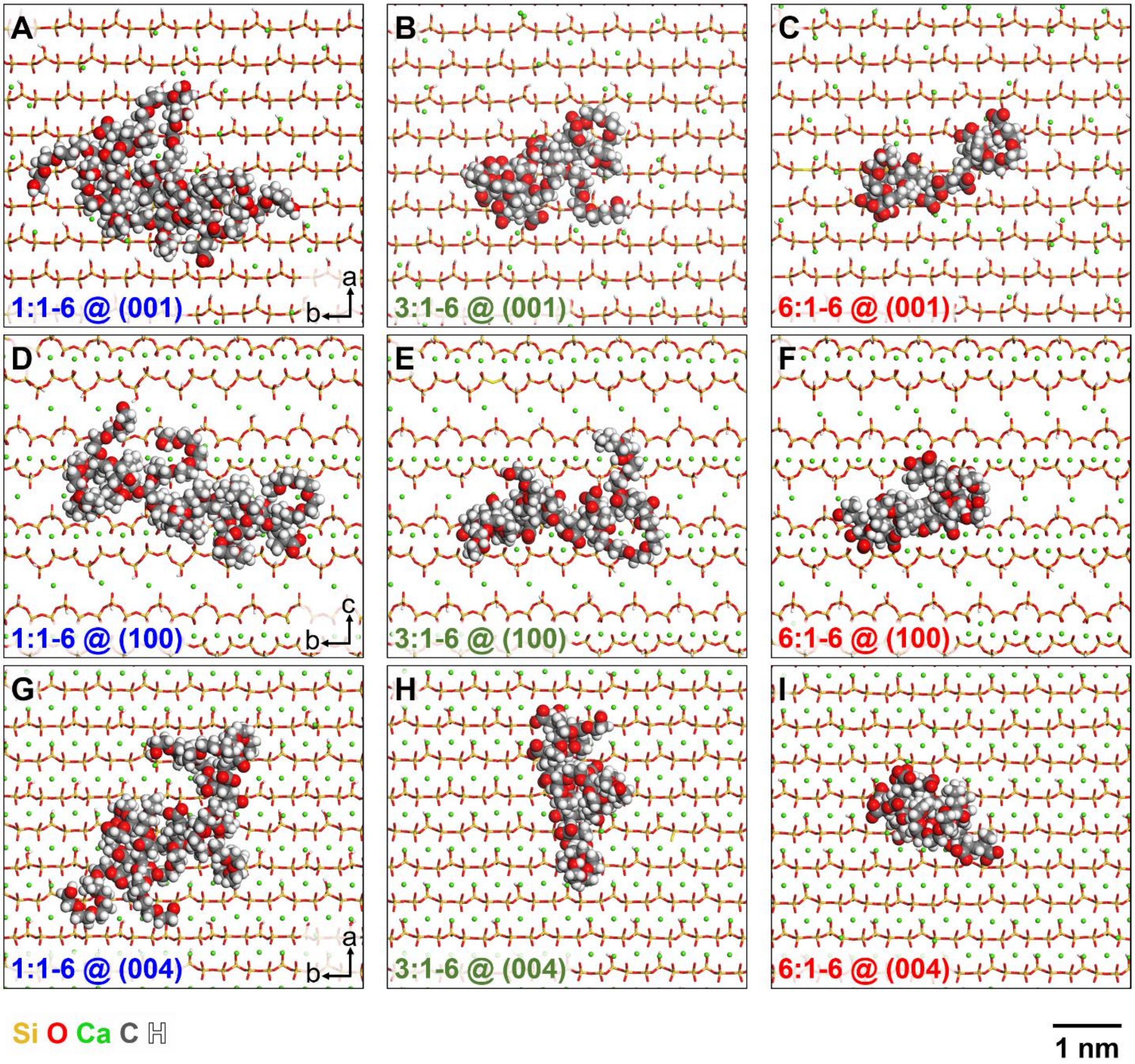

Figure S3. Top view of adsorbed conformation of PCEs with medium long side chains to the C-S-H model surfaces. Only the first atomic layer of the mineral surface is shown for visual clarity. (a-c) Adsorbed conformations on the (001) surface of tobermorite 14 Å. (d-f) Adsorbed conformations on the (100) surface of tobermorite 14 Å. (g-i) Adsorbed conformations on the (004) surface of tobermorite 14 Å. Randomly distributed Ca^{2+} ions between the silicate chains originate from the PCE.

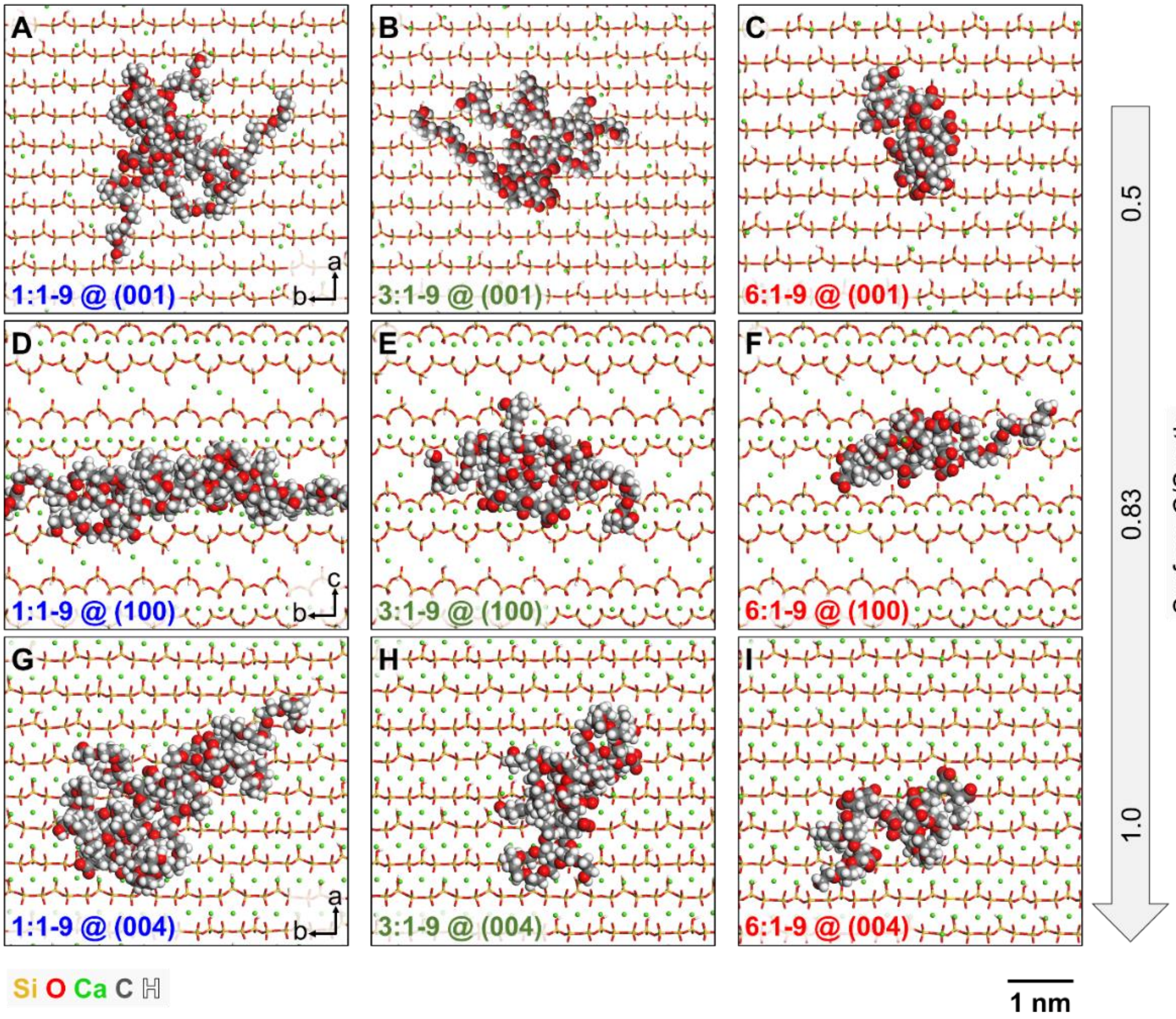

Figure S4. Adsorbed conformation of PCEs with long side chains on the C-S-H model surfaces in top view. Only the first atomic layer of the C-S-H model surface is shown for visual clarity. (a-c) Snapshots on the (001) surface of tobermorite 14 Å. (d-f) Snaphots on the (100) surface of tobermorite 14 Å. (g-i) Snapshots on the (004) surface of tobermorite 14 Å. The occupied surface area per molecule decreases from left (a, d, g) to right (c, f, l) due to lower PEG content and height profiles exceeding 1 nm. Ca^{2+} ions from the polymer backbone are randomly distributed on all surfaces near the PCE molecules (easier to recognize on (001) and (100) surfaces).

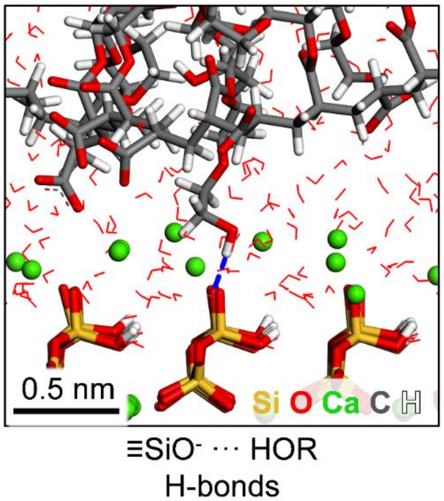

Figure S5. Weak hydrogen bonds between the hydroxyl end group of PEG side chains and siloxide groups ($\equiv SiO^-$) of the tobermorite 14 Å surface, shown for the (001) surface.

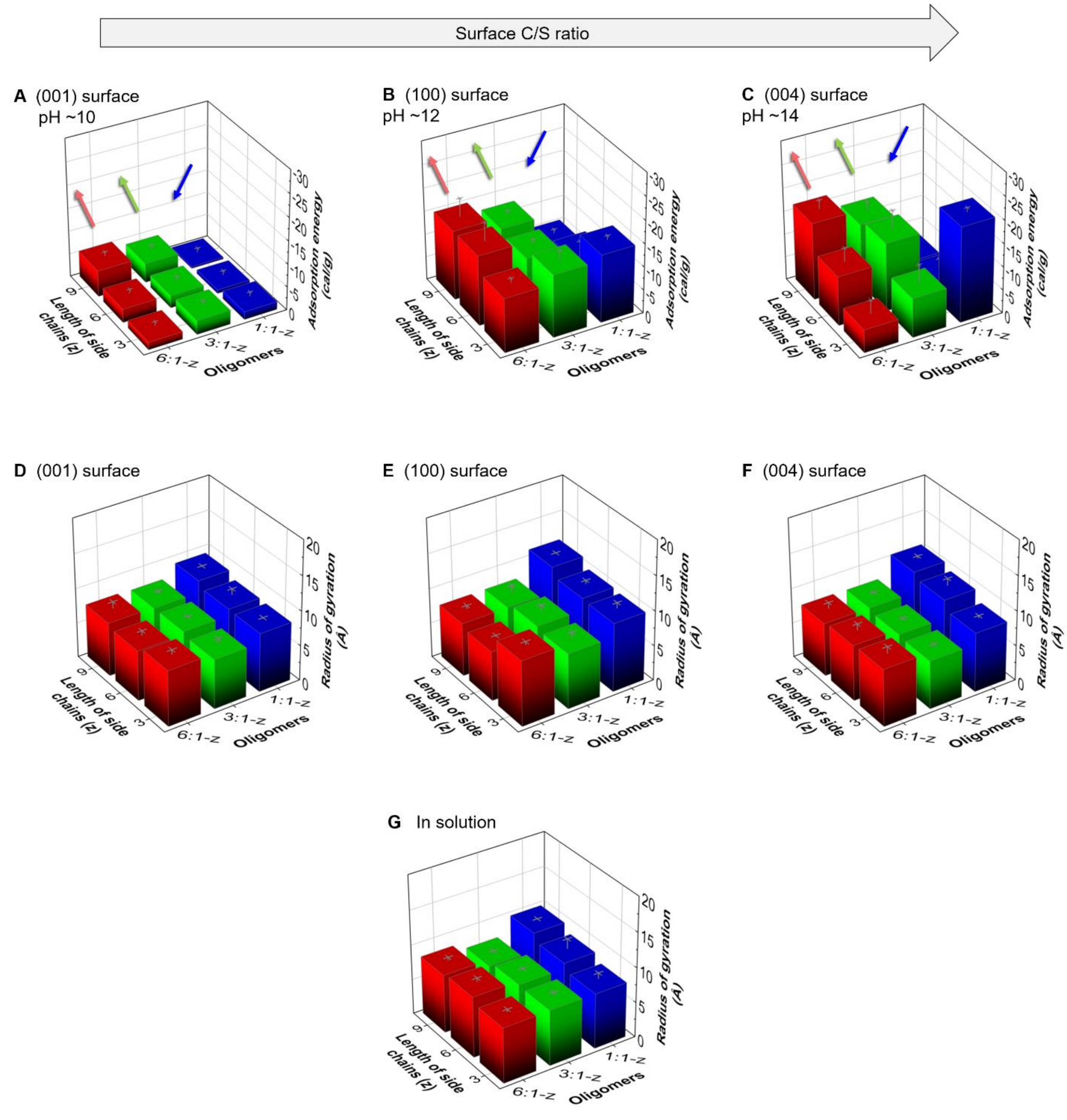

Figure S6. Adsorption energy per unit mass of PCE (in cal/g) and radius of gyration as a function of copolymer structure and C-S-H surface. (a-c) Adsorption energy on the (001) surface, (004) surface, and (100) surface of tobermorite 14 Å. The trend correlates with the adsorption energy per mole. (d-f) Radius of gyration r_g of the 16mer PCE backbone adsorbed on the surfaces. (g) R_g in aqueous solution, away from the surface. The trends in radius of gyration in (d-f) correlate with the trend in end-to-end distances, and the upper limit for a 40 Å long rod-like backbone is $r_g = (1/12)^{1/2} L = 11.5$ Å.

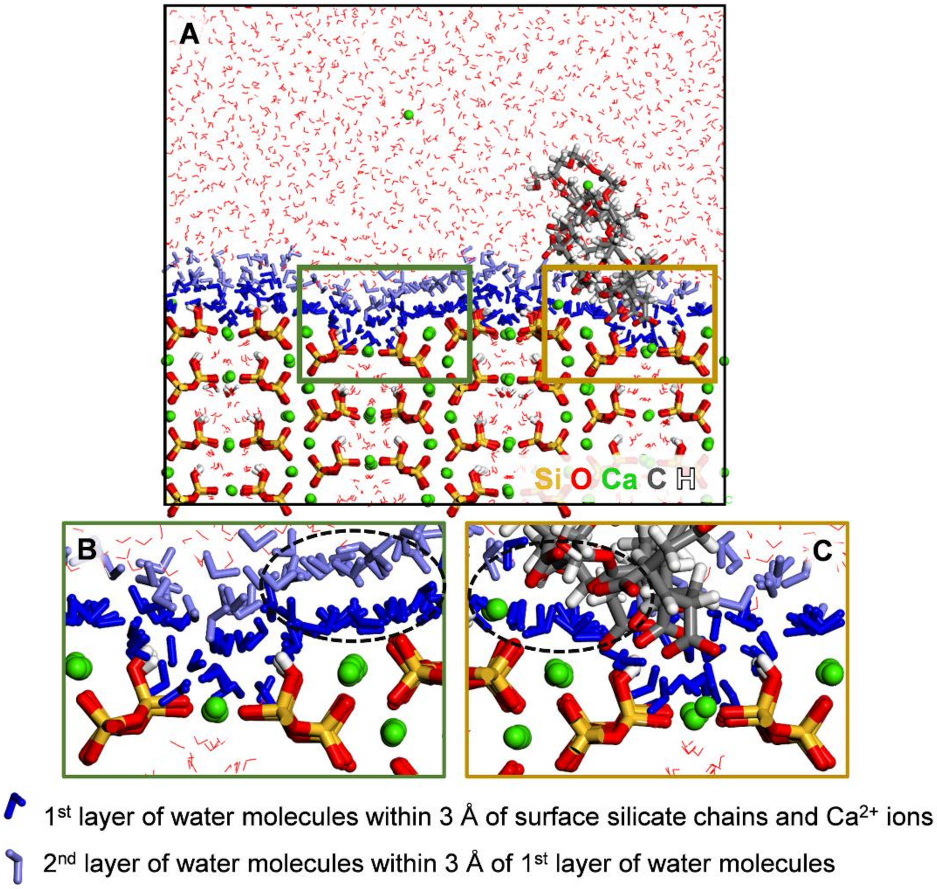

Figure S7. (a) Molecular structure of water on the (100) surface of tobermorite 14 Å in the absence and in the presence of adsorbed PCE 6:1-9. Adsorption on the surface strongly affects the first molecular layer of water and fully displaced the second molecular layer. (b, c) Insets of (a) show the structure of water without and with PCE respectively. Surface layering and replacement of water by PCE 6:1-9 is stronger than on (001) and (004) surfaces and leads to a positive entropy change upon adsorption, i. e., the free energy of adsorption has a significantly larger negative value than the energy of adsorption.

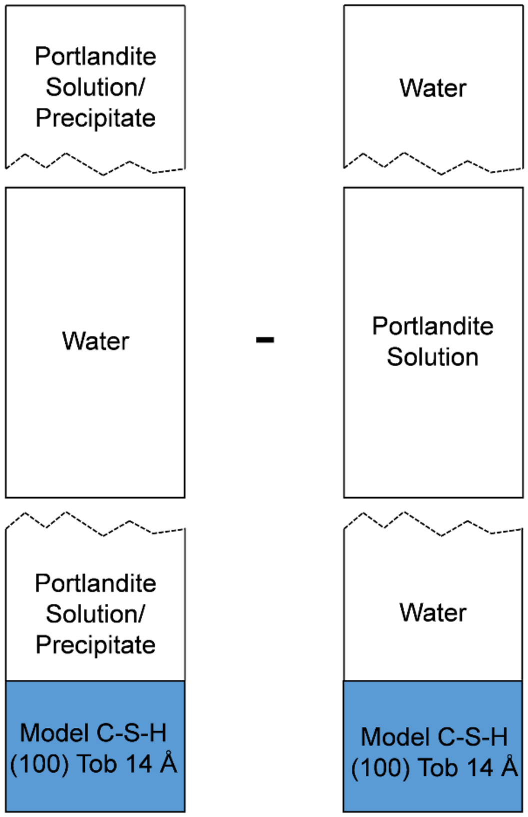

$$E_{ads} = \left(E_{surf+sol} + E_{w}\right) - \left(E_{surf+w} + E_{sol}\right)$$

Figure S8. Computation of the adsorption energy of amorphous $Ca(OH)_2$ (portlandite) on the (100) surface of tobermorite 14 Å (E_{ads}). Several independent simulations with different initial concentrations of dissolved portlandite (right hand side) were carried out, including ~0.2 mol/l, ~0.4 mol/l, and ~0.6 mol/l. The computed adsorption energy was -2 to -3 kcal/mol (i. e., per formula unit of $Ca(OH)_2$). The attraction of calcium hydroxide thus tends to be stronger than the average adsorption energy of per monomer unit of PCE.

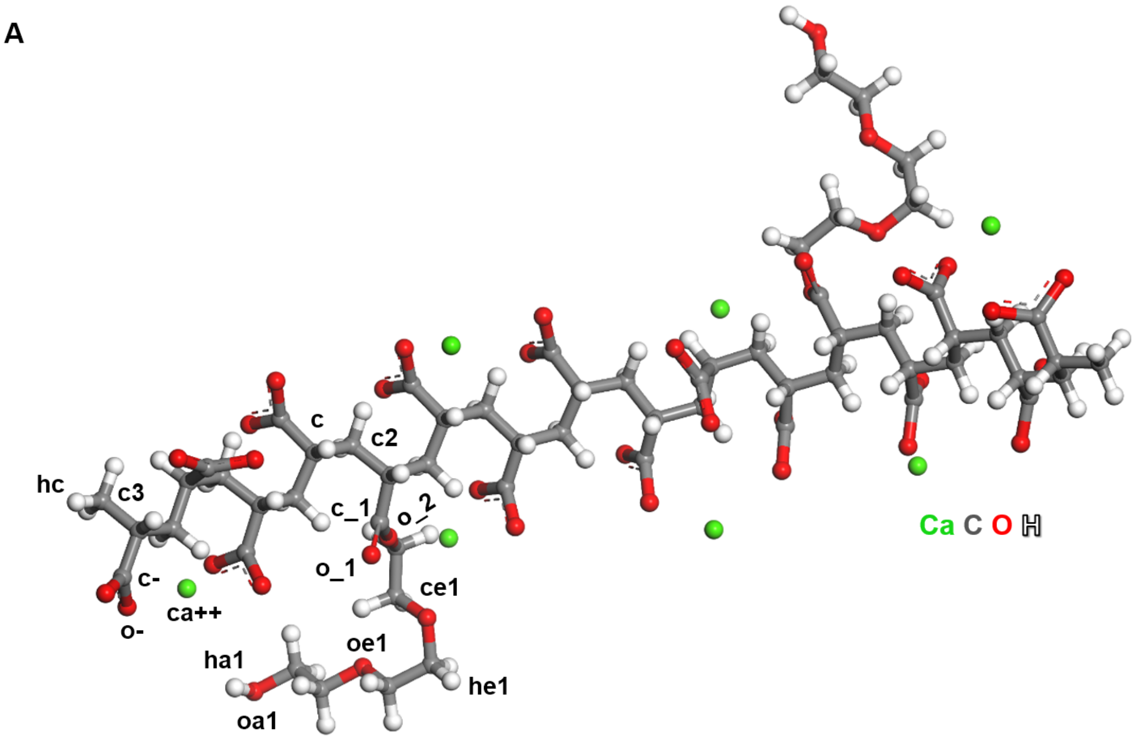

B

Element	C						Ca	H			O				
Atom type	c	c-	c_1	c2	c3	ce1	ca++	ha1	hc	he1	o-	o_1	o_2	oa1	oe1
Atomic charge (e)	-0.053	0.5	0.65	-0.106	-0.159	0.094	1.4	0.4	0.053	0.053	-0.6	-0.45	-0.4	-0.6	-0.4

Figure S9. Element names, atom types and atomic charges for the PCEs as used for the molecular dynamics simulations with PCFF-IFF (version 1.5), shown for a sample structure of PCE 6:1-3 (a) and in table form (b). The other PCEs contain the same functional groups, atoms types, and atomic charges.

A

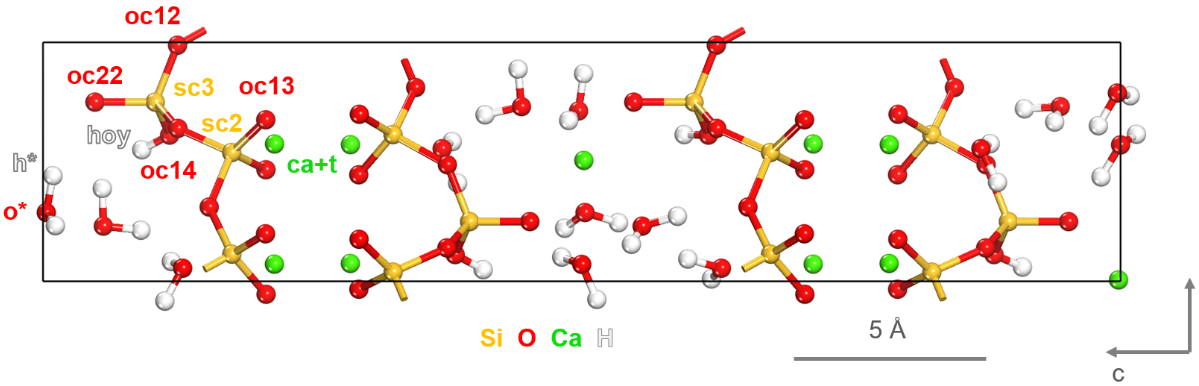

B

Atom type definitions	Atom type ID	Charge (e)	$\sigma_{ii}{}^{a}$ (pm)	$\varepsilon_{ii}{}^{b}$ (kcal/mol)
Ca	ca+t	+1.50	370	0.24
Si (bulk)	sc2	+1.00	420	0.08
Si (silanol)	sc3	+1.00	420	0.08
O (bridge)	oc12	-0.50	365	0.09
O (apical with Ca^{2+} only)	oc13	–1.00	365	0.05
O (apical with Ca^{2+} and water)	oc22	–1.00	370	0.12
O (silanol)	oc14	–0.66	365	0.05
H (silanol)	hoy	+0.41	109.8	0.013
H (flexible SPC water in PCFF)	h*	+0.41	109.8	0.013
O (flexible SPC water in PCFF)	o*	-0.82	361	0.26

[a] Inter-atom distance at which 9-6 Lennard-Jones potential reaches the minimum energy.
[b] Depth of potential well of 9-6 Lennard-Jones potential.

C

Bonds	r_0 (pm)	k_r [kcal/(mol·Å^2)]
sc2 - oc12	169.0	430
sc2 - oc13	162.0	430
sc3 - oc12	169.0	430
sc3 - oc14	168.8	430
sc3 - oc22	163.0	430
oc14 – hoy	94.5	495
o* - h* [a]	97.0	563.28

[a] The parameters for flexible SPC water are the same as in the PCFF force field and listed for completeness only.

Angles	θ_0 (deg)	k_θ [kcal/(mol·rad^2)]
oc12 - sc2 - oc12	100.2	170
oc12 - sc2 - oc13	111.5	170
oc13 - sc2 - oc13	112.5	170
oc12 - sc3 - oc14	111.0	170
oc12 - sc3 - oc12	107.0	170
oc12 - sc3 - oc22	107.0	170
oc22 - sc3 - oc14	111.0	170
sc2 - oc12 - sc3	139.0	170
sc2 - oc12 - sc2	144.0	170
sc3 - oc14 – hoy	125.0	50
h*-o*-h* [a]	103.7	49.84

Figure S10. Atom types, atomic charges, and force field parameters for the tobermorite 14 Å model as used from PCFF-IFF, version 1.5 (ref. [1]). (a) The average unit cell and atom types. (b) Nonbond parameters. (c) Bonded parameters.

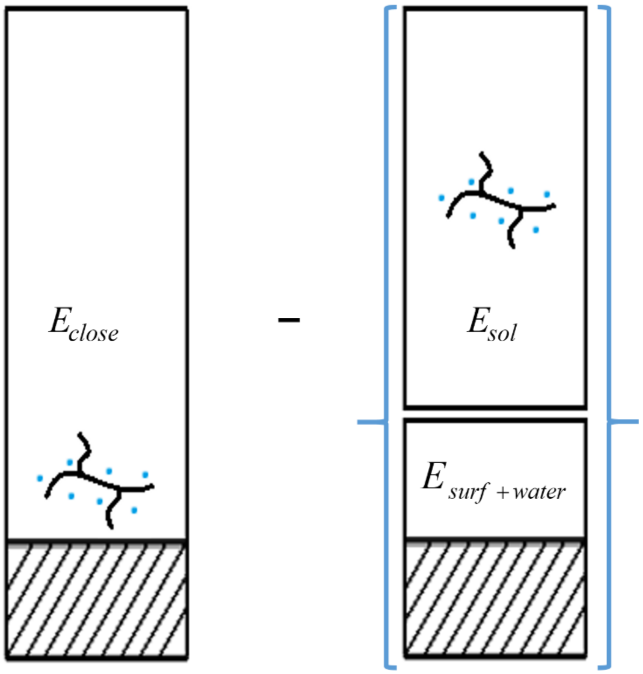

$$E_{ads} = E_{close} - (E_{sol} + E_{surf+water})$$

Figure S11. Method for the calculation of the adsorption energy E_{ads}. The common two-box approach (ref. [2]) was adjusted by splitting the box with desorbed polymer into two additive units, as indicated by blue brackets. E_{close} is the average total energy of the system with the oligomer adsorbed on the tobermorite 14 Å surface, E_{sol} is the average total energy of the system containing water and oligomer only, $E_{surface+water}$ is the average total energy of the system containing a tobermorite 14 Å slab and a thin water slab (about 3 nm) only.

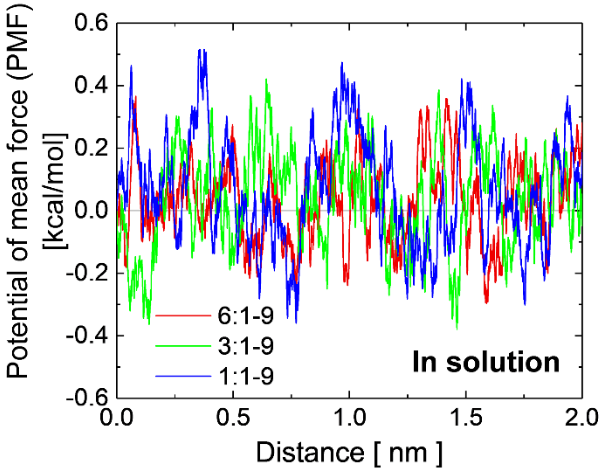

Figure S12. Free energy profile while pulling single PCE oligomers through a dilute aqueous solution, in the absence of a surface, with a constant velocity of 1 nm/ns (time step = 0.5 fs). The cumulative free energy equals the level of background noise (< 0.1 kcal/mol), which is far smaller than the binding free energy to the (hkl) surfaces of tobermorite 14 Å (0 to -80 kcal/mol). Hydrodynamic resistance thus requires only a minimal amount of energy and is practically negligible.

Table S1. Composition and box dimensions of the 3D periodic model systems of polycarboxylate-ether oligomers and tobermorite surfaces used in the molecular dynamics simulations. The dimensions of the solid-liquid interfaces are highlighted in bold.

Oligomer	Tobermorite 14 Å surface	M_r of PCE (g/mol)	No of water molecules	Dimension of tobermorite 14 Å slab (a × b × c) (nm^3)	Total height of simulation box (nm)	Height of surface and water only (nm)
PCE 6:1-9	(001), (004) (100)	2228.5	8,776	**4.51 x 3.71** x 2.80* 2.25 x **2.97 x 5.60**	18.71 18.27	6.73 6.57
PCE 6:1-6	(001), (004) (100)	1964.1	6,727	**3.38 x 4.46** x 2.80 2.25 x **2.97 x 5.60**	16.38 14.55	6.73 6.57
PCE 6:1-3	(001), (004) (100)	1699.8	5,556	**3.38 x 3.71** x 2.80 2.25 x **4.46 x 2.80**	16.27 15.81	6.73 6.57
PCE 3:1-9	(001), (004) (100)	2983.3	11,748	**5.63 x 4.46** x 2.80 2.25 x **4.46 x 5.60**	17.00 16.54	6.73 6.57
PCE 3:1-6	(001), (004) (100)	2454.7	8,407	**4.51 x 4.46** x 2.80 2.25 x **3.71 x 5.60**	15.53 14.55	6.73 6.57
PCE 3:1-3	(001), (004) (100)	1926.1	6,295	**3.38 x 4.46** x 2.80 2.25 x **2.97 x 5.60**	15.52 13.77	6.73 6.57
PCE 1:1-9	(001), (004) (100)	4493.1	17,694	**5.63 x 6.68** x 2.80 2.25 x **6.68 x 5.60**	17.06 16.60	6.73 6.57
PCE 1:1-6	(001), 004) (100)	3435.9	11,767	**5.63 x 5.20** x 2.80 2.25 x **5.20 x 5.60**	15.02 14.55	6.73 6.57
PCE 1:1-3	(001), (004) (100)	2378.6	7,774	**4.51 x 4.46** x 2.80 2.25 x **3.71 x 5.60**	14.48 13.63	6.73 6.57

* Numbers in bold represent the dimensions of the interface in contact with dilute solution of PCE.

Movie Captions

Movie S1. PCE 6:1-9 approaches the (001) surface of tobermorite 14 Å at room temperature during molecular dynamics simulation. Calcium ions bind to the surface first due to faster dynamics, followed by a tail of the polymer and conformation adjustment on the surface.

Movie S2. Adsorbed conformation of PCE 6:1-9 on the (004) surface of tobermorite 14 Å at room temperature during molecular dynamics simulation. The transition between flat-on conformations and locally detached/upright conformations are seen, caused by conformation strain and competition among successive COO^- side groups along the backbone for adsorption sites. The monomer containing a PEG side chain helps both ends of the polymer chain gain contact with the surface.

S1. Computational Methods

S1.1. Models of the Polycarboxylate Ether Oligomers. All-atom models of nine different acrylate-poly(ethylene glycol)acrylate polymers were prepared using the Materials Studio graphical user interface (Figure 1a, b).[3] The models feature acrylate backbones with three different densities of PEG side chains, labeled as PCEs 1:1-z, 3:1-z and 6:1-z, and three different lengths of side chains of z = 3, 6, and 9 ethylene glycol monomers for each backbone configuration. Side chains were grafted via ester linkages and contained a terminal hydroxyl group. We have chosen OH groups to limit the hydrophobic effect of a methyl group, most used in practice, on our oligomers of shorter length than commercial products. In practice, producing such OH terminated groups requires special synthesis routes[4] and commercial products rarely use side chains shorter than 20 units. The length of the backbone was constant at 16 acrylate monomers, with or without PEG, for all nine oligomers. The length is about one fourth of the actual size of polymers typically used in experiments[5] and at the limit of current computing resources for molecular dynamics simulations and conformation sampling in high accuracy. The atom types and atomic charges were assigned according to the PCFF-Interface force field (IFF) which contains accurate parameters for cement minerals, PEG, and acrylate polymers (Figure S9).[1]

S1.2. Models of C-S-H Surfaces. We used the (001), (100), and (004) cleavage planes of the mineral tobermorite 14 Å ($Ca_5Si_6O_{16}(OH)_2 \cdot 7\ H_2O$) as a proxy for surfaces in C-S-H gel (Figure 2a and Figure S10). We employed the average rectangular cell of tobermorite 14 Å provided in the IFF model database as a starting point and then carried out equilibrium cleavage and cation relaxation to create (001), (100) and (004) cleavage planes in equilibrium as described by Fu and Heinz.[6, 7] The area of the cleaved surfaces was customized to approximate the targeted surface coverage of 35% for each PCE (Table S1). We used a mineral slab with a thickness greater than

2.0 nm in all 27 systems to represent the surface of the bulk mineral. IFF reproduces the lattice parameters of tobermorite 14 Å within ~0.5% deviation from X-ray data[8] and the facet-average surface energy of C-S-H ($Ca_3Si_2O_7 \cdot 2H_2O$) in 5% agreement with experimental measurements[9] of 386±20 mJ/m^2 (Figure 2).[1, 10] The majority of surface area is hereby likely composed of the (001) cleavage plane of the lowest surface energy.

An expanded and refined set of IFF parameters and all-atom models for the entire range of tobermorites (9 Å, 11 Å, 14 Å), including both 9-6 and 12-6 Lennard-Jones potentials for PCFF, CHARMM, CVFF, and other force fields will be available soon. Surface and interfacial energies in Figure 2 were computed using this set of parameters. Deviations relative to the current models (Figure S10) are small.

S1.3. Models of the Combined Systems. Models of the combined systems of polymers, C-S-H model surfaces, and water were build using the Materials Studio graphical user interface. We used the flexible SPC water model in the PCFF force field and PCFF-IFF for all simulations. The density of the aqueous solution of the oligomers and of water was set to exactly 1000 kg/m^3 in all systems (Figure S11). The dimensions of the cross-sectional interface were chosen to represent ~35% surface coverage of oligomer in fully stretched conformation in all systems, and this coverage also corresponds to a constant low mass dosage of PCEs (Table S1).[11] Typical box dimensions were 5 × 5 nm^2 laterally and a total box height of 15 nm (Table S1). Two sets of simulation boxes were built for each system, one with the polymer able to bind to the surface (E_{close}), and another with the polymer immersed in solution (E_{sol}) along with a separate surface-water box ($E_{surf+water}$) (Figure S11). In the mineral-polymer-water box, the polymer was initially placed within 4 nm distance away from the surface of the mineral in up to 10 different starting conformations and orientations.

S1.4. Simulation Protocol. The preparation of equilibrium (hkl) cleavage planes[6] and initial energy minimizations of each of the complex interfaces were carried out using the Discover program.[3] Large-scale molecular dynamics simulations were performed using the LAMMPS program.[12] The simulation protocol began with 200 steps further energy minimization, followed by 2000 to 5000 steps of molecular dynamics at 298.15 K in NVT ensemble with a time step of 1 fs to overcome initial close contacts of atoms, for example, between the polymer and added water present in the starting structure in solution and on the surfaces. We then annealed all systems containing the oligomer at 800 K for 6 ns to overcome rotational barriers and effectively sample possible conformation states. Annealing significantly accelerates the path towards equilibrium via time-temperature equivalence.[13] During annealing, we constrained all atoms of the C-S-H surface (when present) except the superficial calcium ions to prevent surface damage.

Subsequently, the system was relaxed at 298.15 K in NVT ensemble for 6 to 12 ns until each replica reached equilibrium as measured by steady total energies. To this point, the summation of Lennard-Jones interactions was carried out using a spherical cutoff of 1.0 nm and the summation of Coulomb interactions with medium accuracy of 10^{-2} using the PPPM solver in LAMMPS. The cut-off for Lennard-Jones interactions was then increased to 1.2 nm and the summation of Coulomb interactions changed to high accuracy of 10^{-6} using the PPPM solver, and the systems subjected to further 2 to 8 ns of molecular dynamics. Average polymer conformation and energies were analyzed for the last 1 to 4 ns of this trajectory. Replicas with apparently higher absolute energy were subjected to a further round of annealing at 400 K for 0.5 ns, followed by relaxation for several nanoseconds at 298.15 K to overcome local equilibria towards the global minimum.

All molecular dynamics simulations were performed using the NVT ensemble, a time step of 1 fs, combination rules and full inclusion of nonbonded interactions between 1,4 bonded atoms as defined in PCFF. All atoms were fully mobile except during annealing as described above.

S1.5. Analysis. Among multiple replicas of the same system, the replicas with the lowest energies were utilized for analysis. Replicas of higher energy (> 10 kcal/mol above the identified minimum) or with positive adsorption energy were discarded, even if contact of oligomer with the surface occurred. First, visual analysis of the trajectories was carried out to examine the interfacial structure and dynamics, the location of the oligomer and the calcium ions, interaction of functional groups with the C-S-H surface, and the preferred conformations of the oligomers. The percent contact time of each oligomer was computed from the last 1 to 4 ns of the equilibrium trajectories using at least 1000 snapshots. The oligomer was considered to be in contact with the C-S-H surface in a given snapshot if any atoms were within 1.0 nm distance from basal oxygen atoms of the C-S-H surface. This distance was chosen larger than usual (0.3 nm) as some PCEs showed steady binding at several Angstrom distance from the surface (PCEs 1:1-9 and 1:1-6 on (001) and (004) surfaces). Adsorption energies E_{ads} were calculated using a modified two-box method with oligomer in close and away states with respect to the surface (Figure S11):[2]

$$E_{ads} = E_{close} - (E_{sol} + E_{surf+water}) \tag{S1}$$

Time-average energies of the major portion of the equilibrated trajectory (30%-70%) were used for obtaining the values of E_{close}, E_{sol} and $E_{surf+water}$. At least five starting conformations (replicas) of each oligomer in “close” configuration were considered to evaluate convergence of the total energy and conformations. All average energies were corrected for the reference temperature (298.15 K) using the heat capacity of the respective system. Uncertainties were determined from differences in the block averages and across multiple replicas.

End-to-end lengths of the PCE backbones were analyzed throughout the equilibrium portion of the trajectories and are reported as an average with standard deviations based on block averages of major portions of the trajectories used for averaging (Figure 8). Similarly, instantaneous coordinates throughout the equilibrium portions of the trajectories were used to compute radii of gyration r_g (considering the backbone only for ease of comparison), starting with the center of mass r_c and applying the definition (Figure S6):

$$r_g^2 = \frac{\sum_{i=1}^{N} m_i (\vec{r}_i - \vec{r}_c)^2}{\sum_{i=1}^{N} m_i} . \tag{S2}$$

Density profiles and radial distribution functions were computed using the same trajectory data of coordinates and applying the definition.

S1.6. Free Energy Calculations. The free energy of binding of PCEs with z = 9 was estimated as a function of the density of the side chains on the three different C-S-H model surfaces using steered molecular dynamics (SMD) (Figure 9).[14, 15] Three independent start configurations were chosen for each system from the available NVT equilibrium trajectories of the lowest energy. The 'fix SMD' command in the LAMMPS program was used to steer the oligomers away from the surface, restarting from the last known velocity distribution in the NVT ensemble. The adsorbed oligomer was pulled from the center of the backbone at a constant velocity of 1 nm/ns in time steps of 0.5 fs over a distance of 4 nm (Figure 9e). The spring constant was 20 kcal/(mol·A^2). For each system, the first cumulants of the potential of mean force were recorded and all three independent energy profiles averaged (Figure 9a-c). The second-order expansion of the Jarzynski's equality was also computed and no noticeable differences were found.[14, 15] To assess the background energy from hydrodynamic resistance, we pulled the oligomer using the same SMD protocol in dilute solution for 2 nm and the free energy contribution from the average profiles was negligible (Figure 9d and Figure S12). The calcium ions associated with the backbone were incompletely desorbed from the surface, however, and the free energies of binding could therefore only be estimated by extrapolation (dashed lines in Figure 9a-c).

S1.7. Adsorption of Multiple PCE Molecules and Calcium Hydroxide. To probe the assembly of multiple PCEs of low density of side chains, simulations of three PCE 6:1-9 oligomers were carried out on the (001) tobermorite 14 Å surface. The dimensions were 5.63 x 6.68 nm^2 (slab thickness 2.80 nm) with a total height of the simulation box of 17.16 nm and 17,694 water molecules, which allows up to 50% surface coverage. The simulation protocol was the same as for the systems with one oligomer and five different independent start conformations were employed.

The adsorption of amorphous calcium hydroxide onto the C-S-H surface was analyzed using simulation boxes with calcium hydroxide (Portlandite) in solution versus adsorbed/precipitated on the (100) tobermorite 14 Å surface using at least 10 ns molecular dynamics simulation (Figure S8).

S1.8. Error Analysis. The major source for uncertainties in computed adsorption energies and adsorption free energies is limited conformation sampling, i. e., the identification of global minima for PCE conformations in solution and on the surface rather than local metastable states. Thermal fluctuations affect the results to a smaller extent. To keep uncertainties low, we restricted the chain length and molecular weight of the model systems as sampling becomes exponentially more difficult for longer chains. We utilized multiple replicas and annealing to overcome energy barriers.[16-18] Uncertainties were quantified as standard deviations of the block average energies in individual, independent simulations relative to the average energy. Adsorption energies and equilibrium conformations showed good convergence. All data were tested for reproducibility within the given error bars.

S2. Details of the Tobermorite 14 Å Surfaces, Stability at Certain pH Values, and Comparisons to Clay Minerals

Specifically, the tobermorite 14 Å (001) surface has a low C/S ratio of 0.5 and 1.2 Ca^{2+} ions per nm^2, and only ~3% of Ca^{2+} ions dissociate more than 3 Å away from superficial siloxide groups (Figure 1c, f). The area density of silanol groups and siloxide groups equals 2.4 per nm^2 each and corresponds to a pH value of ~10 at the low end for cement dispersions.[19, 20] The (100) surface displays a higher C/S ratio of 0.83 and 2.9 Ca^{2+} ions per nm^2, of which only ~1% dissociate more than 3 Å away from superficial siloxide groups (Figure 1d, g). 1.9 silanol groups and 5.8 siloxide groups are present per nm^2 and the corresponding pH value of ~12 can be representative for cement dispersions. The (004) surface exhibits a C/S ratio of 1.0 and densely packed, tightly bound Ca^{2+} ions with an area density of 4.8 per nm^2 (Figure 1e, h). The surface is entirely covered by 9.6 siloxide groups per nm^2 and virtually no dissociation of Ca^{2+} ions was observed. The surface chemistry corresponds to a pH value of ~14 or greater[20-23] at the high end for cement dispersions.

The relation between increasing area density of cations on the surface and decreasing ability to dissociate in water follows trends on silica[24, 25] and clay mineral surfaces.[26, 27] The low degree of dissociation of Ca^{2+} ions between 0.00 and 0.04 per nm^2 on the tobermorite surfaces is yet much less than 0.2 to 0.8 per nm^2 for Na^+, K^+, and Ca^{2+} ions on silica and clay minerals at pH values of 3 to 9. It appears that the stronger localized cation coordination is a result of the high charge density up to 9.6 monovalent ions per nm^2 (and no less than 2.4 monovalent ions per nm^2) at pH 10 to 14 as well as the pointed localization of negative charge on individual O atoms of silicate chains. Oppositely, in clay minerals, the area density of ions is often less than 1.0 monovalent ions per nm^2 (and rarely above 3 per nm^2),[26, 27] and the negative charge is also delocalized across several atoms at defect sites. Stronger cation coordination and less dissociation also limits unfavorable electrostatic repulsion among negatively charged surface sites on the tobermorite 14 Å surfaces after dissociation occurs.

Previously, parallels of the structure of tobermorite and the structure of clay minerals have been suggested. While there is some similarity, the area density of ions is several times higher for tobermorites as discussed above and also the structure of tobermorite minerals (and C-S-H) departs significantly from that of clay minerals. For example, tobermorite 14 Å has a structure $[\text{I-TTO-OTT-}]_N$ in the *c* direction whereby 'I' represents interlayer cations, 'T' tetrahedral silica layers, and 'O' (pseudo)octahedral cacium oxide layers (Figure 2a). A calcium interlayer (I) is present in the (001) and (002) planes, followed by multiple tetrahedral silica (T) and octahedral calcium oxide (O) layers, and a mostly non-covalent junction between O layers. Clay minerals such as montmorillonite, in contrast, have a simple $[\text{I-TOT-}]_N$ structure, no double tetrahedral layers, no double octahedral layers, nor a noncovalent junction between octahedral layers, and display a 6-fold coordination number in the octahedral layer rather than 7-fold in case of tobermorites.[26-28] These differences are significant and lead to very different interfactions with surfactants and polyelectrolytes.

S3. Additional Discussion of Binding Energy and Adsorbed Conformation

The range of adsorption energies per 16mer acrylate at ~35% surface coverage is from -2 kcal/mol to -49 kcal/mol (Figure 8a-c) and similar trends are observed when the adsorption energy is expressed per unit mass (in cal/g) instead of per mole (Figure S6). Adsorption is notably weaker on (001) surfaces with a low C/S ratio of 0.5 in comparison to (100) and (004) surfaces with C/S ratios of 0.83 and 1.0 (Figure 1). The low C/S ratio on the (001) surface (Figure 1c) provides less binding sites for the Ca^{2+} ions and the associated acrylate backbone, resulting in low binding energies. A higher C/S ratio and more than twice the number of calcium ions per nm^2 on the (100) surface augment the adsorption energies relative to the (001) surface by more than 3-fold. The (004) surface with an even higher surface C/S ratio and 4 times the Ca^{2+} area density compared to the (001) surface shows a similar magnitude of adsorption energies as the (100) surface, as well as more differentiation depending on the polymer structure. The protonation state then corresponds to a high pH value of about ~14 relative to a typical pH value of ~13 during cement hydration. The (100) surface with a surface C/S ratio of 0.83, equivalent to a bulk C/S ratio between 1.25 and 1.6, and a pH value of ~12 similar to pore solutions is likely the closest approximation of C-S-H surfaces formed upon hydration of Portland cement, in combination with the (004) surface.

An increase in the length of side chains leads to stronger flat-on binding of PCEs at low (6:1-z) and medium (3:1-z) fractions of side chains, represented by larger negative binding energies approaching up to -40 kcal/mol (red and green arrows in Figure 8a-c). More effective ion-pairing on the surface and less competition from neighbor molecules contribute to the strong binding. A similar increase in binding strength due to backbone conformations occurs for increasing grafting density of short side chains (PCE 6:1-3 to 1:1-3). At a high fraction (1:1) of side chains, however, longer PEG chains reduce accessibility and adsorption of COO^- ions to the surface so that contact time and binding energy decrease to -2 kcal/mol (blue arrows in Figure 8a-c). This decrease in adsorption is caused by more strained, unfavorable flat-on conformations. The differences are especially high on the (004) surface, which has the highest density of potential binding sites for Ca^{2+} ions and anionic acrylate groups. For example, PCEs 6:1-9, 3:1-6, and 1:1-3 contain about the same volume fraction of PEG and, given an abundance of binding sites, the binding enthalpy is about the same (-40 kcal/mol) as shielding between neighbor acrylate backbones by PEG and effects on surface binding are similar (Figure 8c, Figure 6i, Figure S1h, Figure 5g). In contrast, PCEs 6:1-3 and 3:1-3 form weaker ion pairs with the surface and have more ionic interactions with neighbor molecules that could result in a more cohesive organic layer at higher surface coverage (Figure 8c, Figures 5i, Figure 5h).

PCEs 1:1-*z* and partly the PCEs 3:1-z have a high fraction of side chains, rigid backbone conformations, and slow rotational motion (Figure 5a, d, g, Figure 6a, d, g, Figure S1a, d, g, Figures S2-S4a, d, g). Adsorbed conformations are mainly flat-on, residence times often below 100%, and binding energies weak except when the side chains are short (Figure 8a-c). The negatively charged COO^- groups often have an imperfect match with the surface pattern of Ca^{2+} ions due to conformation strain in the backbone. The PCEs in flat-on conformations, or nearly flat-on conformations, also showed an orientation preference parallel to the silicate chains on the tobermorite 14 Å surfaces (Figures S2, S3, and S4). PCEs 3:1-*z* and 6:1-*z* have a lower fraction of side chains, more conformational flexibility of the backbone, and faster rotational motion, for example, PCE 3:1-3 (Figure 5b, e, h) and PCE 6:1-9 (Figure 6c, f, i, Figure S4c, f, i). Adsorbed conformations are typically tilted relative to the surface, contact with the C-S-H surface is permanent, and binding energies are strong (Figure 8a-c).

A higher fraction of side chains in PCEs 1:1-z leads to more surface-selective binding as shown by larger differences in adsorption enthalpy and in contact time on the different (hkl) surfaces compared to other polymers (Figure 8a-c as well as Figures 5, 6, and Figure S1). The PCEs 1:1-3, 1:1-6, and 1:1-9 show distinct binding energies to all surfaces, for example, a marked increase from (001) to (100) to (004) for z = 3. The reason are strained flat-on conformations with limited conformational flexibility, which result in a good or poor fit and less adaptability to the surface (Figures 5 and 6). In contrast, the 6:1-*z* polymers, and partly the 3:1-*z* polymers, possess more potential COO^-/Ca^{2+} sites for binding along the backbone and can better adapt their conformation to a given C-S-H surface due to higher conformational flexibility. While adsorption is distinctively weaker on (001) surfaces, the trends on (100) and (004) surfaces are similar.

A particular case is observed on the (004) surface, where no hydrogen bond with the surface is possible and where the PCE 6:1-3 oligomer (highest charged oligomer) has an adsorption energy 5 times less than the 1:1-3 oligomer (Figure 8c). Here, the 1:1-3 oligomer is rather effective in coordinating surface calcium ions without conformation hindrance, i. e., without repulsion by more than 2 successive COO^- groups. The 6:1-3 oligomer has too many successive CO_2^- groups to bind to the highly charged surface, and the short side chains allow more globular conformations that reduce adhesion. However, the situation might be different for 10 times higher PCE coverage on the surface. Then, the stickiness of the oligomers to each other determines the stability of the polymer film, provided some basic adhesion to the C-S-H surface that is present in all cases according to the simulation. Then, 6:1-z oligomers likely have more ionic cohesion among each other than the 1:1-z oligomers and could form a more adhesive polymer film. In contrast, the 1:1-z oligomers would have less inter-chain ionic attraction and likely bind less.

To ease comparisons to future experiments, the adsorption energies are reported in kcal/mol (Figure 8) and also in calories per gram (cal/g), which accounts for differences in molecular weight and is also commonly used to assess the binding energy per mass of additive (Figure S6). While the trends are the same, molecules of higher molecular weight (e.g., PCE 1:1-9) have reduced adsorption energies per gram and molecules of lower molecular weight (e.g., PCE 6:1-9) show larger adsorption energies per gram. The different unit only normalizes per weight of PCE instead of the number of moles. All data correspond to equal mass dosage of ~0.4 mg PCE per g of cement since constant surface coverage equals constant mass dosage. Our surface coverage of ~35% in all cases was defined as occupied surface area by available surface area, assuming flat-on conformations (see main text).

S4. Additional Discussion of Binding Free Energy

Free energies of adsorption for PCE 6:1-9 and PCE 3:1-9 on (100) surfaces, which are suitable regular models for amorphous C-S-H surfaces in cement, amount to about twice the adsorption energy (Figure 9b) and identical values are obtained for PCE 1:1-9. Then, the entropy gain of water outweighs the entropy loss of binding PCEs 6:1-9 and 3:1-9, even given uncertainty due to surface-bound cations. Further analysis of the bound states reveals that the strongly ionic polymers PCEs 6:1-9 and 3:1-9 penetrate two well-structured, confined molecular water layers specific to the (100) surface, which explains a large entropy gain upon adsorption (Figure S5). Such tight binding does not occur on the (004) surface at pH ~14, and not on the (001) surface at pH ~10. On the (100) surface at pH ~12, also silanol groups contribute significantly to the decrease in free energy of binding by constraining the conformational freedom of oligomer backbone from multiple points with the formation of $\equiv$SiO**H** ⋯ $^{-}$**O**OC-R hydrogen bonds. The gain in free energy (relative to the energy) is up to ~ -0.75 kcal/mol for each replaced water molecule, using a portion of the enthalpy of melting from fully immobilized ice to liquid of -1.435 kcal/mol,[29] and the involvement of up to 60 water molecules per PCE oligomer can explain differences up to -40 kcal/mol. The carboxylate groups in the six times less ionic polymer 1:1-9 do not approach the surface as closely, leading to a less significant entropy contribution (Figure 6d-f).

The trends in adsorption free energy suggest remote relationships to the role of PCEs in the initial hydration of cement particle surfaces (apart from hydration of C_3A and formation of ettringite). Initial hydration of C_3S surfaces involves the protonation of superficial oxide and silicate ions.[30, 31] During this process, the pH value of the system almost immediately jumps to about pH ~ 13, whereby very initial C_3S and C_3A surfaces with oxide and hydroxide ions may cause locally higher pH values than 14.[23] According to the simulation, typical PCEs x:1-9 adsorb weaker at pH values of ~14, represented by the (004) surfaces, and have a much lower free energy of adsorption at pH values near ~12, represented by (100) surfaces (Figure 9a-c). This trend correlates with experimental observations of higher affinity of PCEs to cement particles after 10 to 15 min hydration time compared to immediate addition, which is also dominated by hydration of tricalcium aluminate (C_3A).[32] The higher affinity of these PCEs to C-S-H surfaces at lower pH value is related to the lower cation area density on the surface. In addition to C-S-H phases, also other phases like aluminate and gypsum play a role and could have similar surface coverage but likely different adsorption free energies.

Specifically, sulfate ions from dissolved gypsum in cement compete with PCEs for adsorption due to higher mobility[33-36] and, for a series of different sulfate concentrations in experiments, a higher adsorbed mass was reported for a PCE gradient copolymer compared to PCE random copolymers with the same total number of side chains.[37] We may speculate that the portion of the gradient copolymer with low density of side chains may adsorb stronger on the C-S-H surface between sulfate ions by taking a tilted orientation and could increase the number of molecules adsorbed compared to the random copolymer with a higher average density of side chains. Follow-on studies would be helpful to clarify such complex relationships.

S5. Additional Discussion of Zeta Potentials

A range of observations has been reported for zeta potentials. Some experimental studies report a small negative zeta potential of cement particles, which increases upon addition of PCEs and sometimes reverses to positive values.[38, 39] Also, positive zeta potentials and a decrease to negative values upon addition of PCEs have been reported.[40, 41] Differences in pH value, ion adsorption, and electrolyte composition could explain these data as illustrated in the following examples. (1) Neat tobermorite (or C-S-H) surfaces dissociate calcium ions in an electric field, leading to a small negative zeta potential, which upon adsorption of PCEs is reversed by the proposed mechanism of adsorption of Ca^{2+} ions followed by the negatively charged polymer backbone (Figure 4). Then, the additional calcium ions from the PCE are rather tightly bound to the surface and partial dissociation of the negatively charged polymer in an electric field increases the zeta potential of the cement particle towards a higher positive value. (2) If Na^{+} ions are present on the PCE, rather than Ca^{2+} ions, the Na^{+} ions are less likely to bind to the C-S-H surface and retain a negative zeta potential of the cement particles. The negative zeta potential may be augmented by some bound, negatively charged PCE molecules. (3) Adsorption of large amounts of negatively charged polymer (as a continuous film) can also reduce the zeta potential to negative in case (1), as then only some calcium ions may dissociate from the negatively charged polymer layer on the surface in an applied electric field. (4) Alternatively, in the presence of added $Ca(OH)_2$ or similar electrolytes, additional Ca^{2+} ions may deposit on the C-S-H surface and cause a positive zeta potential, allowing the dissociation of OH^{-} ions under an applied electric field (Figure 10a, c).

Initial addition of PCEs can add to the positive zeta potential and formation of a dense layer cause reversal to negative values as in cases (2) and (3).

S6. Limitations and Opportunities

Limitations of the atomistic models include simplifications regarding the multitude of mineral phases that may be present in cement,[42] the accessible length and time scales, possible electrolyte conditions in the pore solution, assumptions about the molecular weight of the polymers, surface coverage, as well as the reliability of the force fields. Details of the C-S-H models and simplifications of the polymer composition have been described in the main text. We simplified the electrolyte conditions to salt free solution in this first study, including test cases with added $Ca(OH)_2$, and the effects of different electrolyte compositions remain to be explored. Understanding at the single molecule level as presented here provides a foundation for explaining the assembly of more densely packed polymer films. An analysis of the different possible mineral phases, polymer architectures, electrolytes, temperatures, concentrations and more complex organic multilayers would be interesting for future work.

Technical limitations using all-atom models mainly include the accessible time and length scales and related sampling. The accuracy of the force field is likely a smaller source of uncertainty. The lateral dimensions of the simulation box are not a significant constraint here as the low surface coverage leaves room for conformation sampling of the single copolymers and reduces the bias towards correlation with periodic images. Some remaining correlation with periodic images of the charged molecules is also realistic given that the PCE films on cement particles experience major polymer-polymer interactions. The simulation times of tens of nanoseconds are very short compared to experimental relaxation times of seconds to hours, however, they are reasonably long to study the relaxation of single oligomers on the nanoscale and at least 6 orders of magnitude longer than accessible by DFT or other quantum calculations. The study of multilayer polymer films and larger C-S-H morphologies up to the 1000 nm scale is feasible using large-scale computing resources and can be greatly enhanced by complementary experimental measurements.

Supplementary References

1. H. Heinz, T.-J. Lin, R. K. Mishra and F. S. Emami, *Langmuir*, 2013, **29**, 1754-1765.
2. H. Heinz, *J. Comput. Chem.*, 2010, **31**, 1564-1568.
3. *Materials Studio 7.0 Program Suite and User Guide*, Biovia/Accelrys, Inc., Cambridge, UK, 2015.
4. J. Plank, K. Poellmann, N. Zouaoui, P. R. Andres and C. Schaefer, *Cem. Concr. Res.*, 2008, **38**, 1210-1216.
5. F. Winnefeld, S. Becker, J. Pakusch and T. Götz, *Cem. Concr. Compos.*, 2007, **29**, 251-262.
6. Y. T. Fu and H. Heinz, *Chem. Mater.*, 2010, **22**, 1595-1605.
7. Y. T. Fu and H. Heinz, *Philos. Mag.*, 2010, **90**, 2415-2424.
8. E. Bonaccorsi, S. Merlino and A. R. Kampf, *J. Am. Ceram. Soc.*, 2005, **88**, 505-512.
9. S. Brunauer, D. L. Kantro and C. H. Weise, *Can. J. Chem.*, 1959, **37**, 714-724.
10. R. K. Mishra, A. K. Mohamed, D. Geissbühler, H. Manzano, T. Jamil, R. Shahsavari, A. G. Kalinichev, S. Galmarini, L. Tao, H. Heinz, R. Pellenq, A. C. Van Duin, S. C. Parker, R. J. Flatt and P. Bowen, *Cem. Concr. Res.*, 2017, **102**, 68-89.
11. R. K. Mishra, H. Heinz, T. Müller, J. Zimmermann and R. J. Flatt, *American Concrete Institute Symposium Series*, 2012, **288**, 235-251.
12. S. Plimpton, *J. Comput. Phys.*, 1995, **117**, 1-19.
13. K. C. Jha, H. Liu, M. R. Bockstaller and H. Heinz, *J. Phys. Chem. C*, 2013, **117**, 25969-25981.
14. C. Jarzynski, *Phys. Rev. Lett.*, 1996, **78**, 2690-2693.
15. S. Park, F. Khalili-Araghi, E. Tajkhorshid and K. Schulten, *J. Chem. Phys.*, 2003, **119**, 3559-3566.
16. H. Ramezani-Dakhel, L. Y. Ruan, Y. Huang and H. Heinz, *Adv. Funct. Mater.* , 2015, **25**, 1374-1384.
17. I. L. Geada, H. Ramezani-Dakhel, T. Jamil, M. Sulpizi and H. Heinz, *Nat. Comm.*, 2018, **9**, 716.
18. J. R. Gissinger, C. Pramanik, B. Newcomb, S. Kumar and H. Heinz, *ACS Appl. Mater. Interfaces*, 2018, **10**, 1017-1027.
19. S. V. Patwardhan, F. S. Emami, R. J. Berry, S. E. Jones, R. R. Naik, O. Deschaume, H. Heinz and C. C. Perry, *J. Am. Chem. Soc.*, 2012, **134**, 6244-6256.
20. F. S. Emami, V. Puddu, R. J. Berry, V. Varshney, S. V. Patwardhan, C. C. Perry and H. Heinz, *Chem. Mater.*, 2014, **26**, 2647-2658.
21. H. Heinz, *J. Phys.: Condens. Matter*, 2014, **26**, 244105.
22. H. Heinz, *Curr. Opin. Chem. Eng.*, 2016, **11**, 34-41.
23. E. Pustovgar, R. K. Mishra, M. Palacios, J. B. d'Espinose de Lacaillerie, T. Matschei, A. S. Andreev, H. Heinz, R. Verel and R. J. Flatt, *Cem. Concr. Res.*, 2017, **100**, 245-262.
24. K. Haraguchi and H.-J. Li, *Macromolecules*, 2006, **39**, 1898-1905.
25. J. Wu, J. Lin, M. Zhou and C. Wei, *Macromol. Rapid Commun.*, 2000, **21**, 1032-1034.
26. H. Heinz, *Clay Miner.*, 2012, **47**, 205-230.
27. T. Jamil, J. R. Gissinger, A. Garley, N. Saikia, A. Upadhyay and H. Heinz, *Nanoscale*, 2019, **11**, 11183-11194.
28. F. Bergaya and G. Lagaly, *Handbook of Clay Science*, Elsevier, Amsterdam, 2013.
29. M. Turesson, C. Labbez and A. Nonat, *Langmuir*, 2011, **27**, 13572-13581.

30. H. Taylor, P. Barret, P. Brown, D. Double, G. Frohnsdorff, V. Johansen, D. Ménétrier-Sorrentino, I. Odler, L. Parrott and J. Pommersheim, *Mat. Constr.*, 1984, **17**, 457-468.
31. P. Barret, D. Ménétrier and D. Bertrandie, *Cem. Concr. Res.*, 1983, **13**, 728-738.
32. N. Roussel, *Understanding the Rheology of Concrete*, Elsevier Science, 2011.
33. J. Cheung, A. Jeknavorian, L. Roberts and D. Silva, *Cem. Concr. Res.*, 2011, **41**, 1289-1309.
34. S. Han and J. Plank, *Adv. Cem. Res.*, 2013, **25**, 200-207.
35. F. Dalas, A. Nonat, S. Pourchet, M. Mosquet, D. Rinaldi and S. Sabio, *Cem. Concr. Res.*, 2015, **67**, 21-30.
36. K. Yamada, S. Ogawa and S. Hanehara, *Cem. Concr. Res.*, 2001, **31**, 375-383.
37. S. Pourchet, S. Liautaud, D. Rinaldi and I. Pochard, *Cem. Concr. Res.*, 2012, **42**, 431-439.
38. A. Zingg, F. Winnefeld, L. Holzer, J. Pakusch, S. Becker, R. Figi and L. Gauckler, *Cem. Concr. Compos.*, 2009, **31**, 153-162.
39. J. Plank, R. Schwerd, D. Vlad, A. Brandl, and P. Chatziagorastou, *GDCh-Monographie Band*, 2004, **31**, 58-69.
40. O. Akhlaghi, Y. Z. Menceloglu and O. Akbulut, *Sci. Rep.*, 2017, **7**, 41743.
41. L. Ferrari, J. Kaufmann, F. Winnefeld and J. Plank, *J. Colloid Interface Sci.*, 2010, **347**, 15-24.
42. H. F. W. Taylor, *Cement Chemistry*, Academic Press, London, 1997.